

Supplementary Information

Plasmonic Bi NPs-accelerated interfacial charge transfer for enhanced solar-driven ciprofloxacin mineralization

Cailiang Yue ^a; Changqing Zhu ^a; Wenting Zheng ^a; Jinli Qiu ^a; Zhiling Du ^a; Chen
Ling^b; Fu-Qiang Liu ^{a, *};

^a *State Key Laboratory of Pollution Control and Resource Reuse, School of the
Environment, Nanjing University, Nanjing 210023, Jiangsu, P.R. China*

^b *College of Biology and the Environment, Nanjing Forestry University, Nanjing
210037, Jiangsu, P.R. China*

*** Corresponding Author**

**Phone: +86 139 1387 1032; E-mail: lfq@nju.edu.cn (Fu-Qiang Liu)*

Txt S1. Preparation of photocatalysts

Preparation of Bi NPs. Bi NPs was synthesized via simple solvothermal method. Generally, 4 mmol $\text{Bi}(\text{NO}_3)_3 \cdot 5\text{H}_2\text{O}$ was dissolved in 40 mL ethylene glycol with slowly stirring for 1 h. Afterwards, the solution was transferred into a 100 mL Teflon-lined stainless-steel autoclave and solvothermally treated at 200 °C for 12 h prior to natural cooling to room temperature. The obtained powder was centrifuged, washed thrice with ultrapure water and dried at 200 °C for 12 h.

Preparation of Bi_2MoO_6 and BiOBr. Bi_2MoO_6 and BiOBr were synthesized by solvothermal method. Firstly, 4 mmol $\text{Bi}(\text{NO}_3)_3 \cdot 5\text{H}_2\text{O}$ was dissolved in 40 mL ethylene glycol to obtain solution A. 4 mmol NaBr and 2 mmol Na_2MoO_4 were dissolved in 10 mL ethylene glycol to obtain solution B. Subsequently, solution B was dropped into solution A with slowly stirring for 1 h. Then, the mixed solution was transferred into a 100 mL Teflon-lined stainless-steel autoclave and solvothermally treated at 140 °C for 12 h prior to natural cooling to room temperature. The obtained powder was centrifuged, washed three times with ultrapure water and dried at 60 °C for 12 h. The obtained Bi_2MoO_6 and BiOBr were named as BMO and BOB, respectively.

Preparation of Bi/ Bi_2MoO_6 and Bi/BiOBr. The synthesis of Bi/ Bi_2MoO_6 and Bi/BiOBr were similar to that of BMO and BOB, except that the solvothermal temperature was adjusted to 200 °C.

Preparation of $\text{Bi}_2\text{MoO}_6/\text{BiOBr}$. For comparison, binary heterojunction $\text{Bi}_2\text{MoO}_6/\text{BiOBr}$ with optimized molar ratio ($\text{NaBr}:\text{Na}_2\text{MoO}_4=2:1$) was also prepared. Generally, 4 mmol $\text{Bi}(\text{NO}_3)_3 \cdot 5\text{H}_2\text{O}$, 2 mmol NaBr and 1 mmol Na_2MoO_4 was dissolved in 40 mL ethylene glycol with slowly stirring for 1 h. Then, the solution was transferred into a 100 mL Teflon-lined stainless-steel autoclave and was solvothermally treated at 140 °C for 12 h and followed by natural cooling to room temperature. The obtained powder was centrifuged, washed three times with ultrapure water and dried at 60 °C for 12h. The obtained $\text{Bi}_2\text{MoO}_6/\text{BiOBr}$ was named as BMO/BOB.

Table S1. The synthesis conditions of different photocatalysts.

Photocatalysts	Temperature & Time	Bi(NO₃)₃	NaBr	Na₂MoO₆
Bi	200 °C/24 h	4 mmol	0	0
BMO	140 °C/24 h	4 mmol	0	2.0 mmol
BOB	140 °C/24 h	4 mmol	4 mmol	0
Bi/BMO	200 °C/24 h	4 mmol	0	2.0 mmol
Bi/BOB	200 °C/24 h	4 mmol	4 mmol	0
BMO/BOB	140 °C/24 h	4 mmol	2 mmol	1.0 mmol
BMO/Bi/BOB-1	200 °C/24 h	4 mmol	3 mmol	0.5 mmol
BMO/Bi/BOB-2	200 °C/24 h	4 mmol	2 mmol	1.0 mmol
BMO/Bi/BOB-3	200 °C/24 h	4 mmol	1 mmol	1.5 mmol

Table S2. Analysis parameters for representative organic pollutants.

	SMZ	TC	BPA	Phenol
Instrument	HPLC, LC-2030C, Shimadzu			
Column	C18 column (4.6 μ m, 2.1 mm \times 250 mm)			
Injection volume (μL)	10			
Flow rate (mL/min)	1			
Mobile phase	Mobile phase A: H ₂ O (0.5wt% KH ₂ PO ₄) Mobile phase B: 100% Acetonitrile	Mobile phase A: H ₂ O (0.5wt% NaH ₂ PO ₄) Mobile phase B: 100% Acetonitrile	Mobile phase A: 100% Methanol Mobile phase B: 100% H ₂ O	Mobile phase A: 100% Methanol Mobile phase B: 100% H ₂ O
Elution program	Gradient: 60% Mobile phase A 40% Mobile phase B	Gradient: 75% Mobile phase A 25% Mobile phase B	Gradient: 70% Mobile phase A 30% Mobile phase B	Gradient: 80% Mobile phase A 20% Mobile phase B
Detector	UV detector			
Wavelength	270 nm	358 nm	275 nm	224 nm

Table S3. BET surface and porosity parameters of BOB, BMO, BMO/BOB and BMO/Bi/BOB-2.

Sample	S_{BET} (m²·g⁻¹)	Micropore volume (cm³·g⁻¹)	Average pore diameter (nm)
BOB	7.91	0.09	30.21
BMO	8.32	0.08	24.49
BMO/BOB	20.03	0.07	8.33
BMO/Bi/BOB-2	28.84	0.06	7.02

Table S4. Bi specie content (Atom ratio%) of BMO/Bi/BOB-2.

Bi 4f	Area ratio (%)
Bi³⁺	89.25
Bi⁰	10.75

Table S5. Comparison of photocatalytic CIP degradation over recently reported photocatalysts.

Photocatalysts	Dosage (g/L)	Concentration (mg/L)	Light source	k value (min ⁻¹)	TOC removal (%)	Refs.
Zn doped Cu ₂ O	0.6	20	500 W metal halide lamp	0.0038	-	1
TiO ₂ /γ-Fe ₂ O ₃ /GO	0.4	10	300W Xe light	0.0048	49.0% in 160 min	2
γ-Fe ₂ O ₃ @ZnO	0.5	10	300W Xe light	0.0843	-	3
N-doped TiO ₂	0.5	10	Blue LED light	0.0093	-	4
BiOCl/diatomite	0.5	10	300W Xe light	-	42.9% in 240 min	5
Bi ₂ O ₃ /(BiO) ₂ CO ₃	0.5	10	300W Xe light	0.1170	21% in 240 min	6
Br doped Bi ₂ O ₃ CO ₃	0.5	10	240W Xe light	0.0860	43% in 30 min	7
Bi/Bi ₃ NbO ₇	0.5	10	300W Xe light	0.0143	53% in 180 min	8
rGO/Fe ₂ O ₃ /g-C ₃ N ₄	1	50	500W halogen lamp	0.0836	-	9
TP-TiO ₂	0.1	10	UV-vis light	0.0403	-	10
P25	0.1	20	LED	0.2217	62.7% in 40 min	11
Mn ₂ O ₃ /Mn ₃ O ₄ /MnO ₂	0.2	10	300W Xe lamp	-	78.3% in 40 min	12
Ag ₂ CrO ₄ /Ag/BiFeO ₃ @RGO	0.2	10	350W Xe light	0.0638	78.3% in 120 min	13
This work	0.4	20	350W Xe light	0.1389	79.9% in 120 min	-

Table S6. The recovery rates and Bi leaching on each cycle.

	1st	2nd	3rd	4th	5th
Recovery rate (%)	100	97.61	96.17	94.62	93.07
Bi leaching (mg/L)	0.093	0.089	0.076	0.070	0.072

Table S7. Fitting parameters for TRPL of prepared photocatalysts.

Fitting parameters	τ_1 (ns)	τ_2 (ns)	B₁	B₂	τ_{average} (ns)
BOB	2.58	65.52	2045.73	348.17	53.69
BMO	2.42	55.12	2194.34	328.64	43.61
BMO/BOB	2.41	115.09	2664.32	90.73	72.18
BMO/Bi/BOB-2	2.29	135.12	2754.34	78.64	85.51

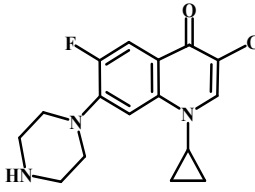
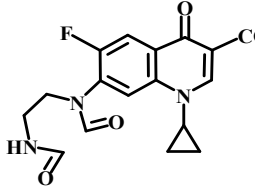
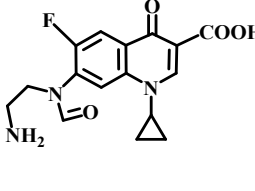
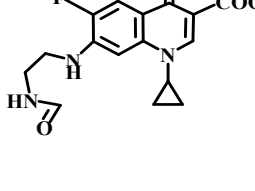
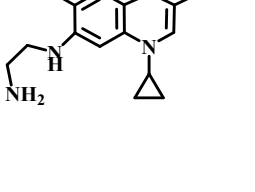
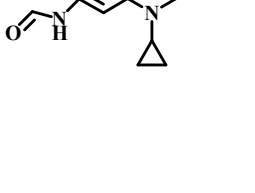
Time-resolved fluorescence decay spectra of BMO, BOB, BMO/BOB and BMO/Bi/BOB-2 were determined at 475, 441, 465 and 455 nm respectively under the incident light of 325 nm. The decay curves could be fitted based on the following equation.

$$I = B_1 \exp(-t/\tau_1) + B_2 \exp(-t/\tau_2) \quad \text{Eq. S1}$$

The average lifetime was calculated by using the following equation.

$$\tau_{\text{average}} = (B_1 \tau_1^2 + B_2 \tau_2^2) / (B_1 \tau_1 + B_2 \tau_2) \quad \text{Eq. S2}$$

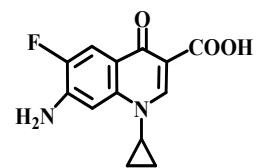
Table S8. The structural information of CIP and the possible intermediates.

Compounds	Formula	m/z	Proposed structure
CIP	$C_{17}H_{18}FN_3O_3$	332	
I 1	$C_{17}H_{16}FN_3O_5$	362	
I 2	$C_{16}H_{16}FN_3O_4$	334	
I 2'	$C_{16}H_{16}FN_3O_4$	334	
I 3	$C_{15}H_{16}FN_3O_3$	306	
I 4	$C_{15}H_{15}FN_2O_3$	291	

I 5



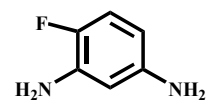
263



I 6



126



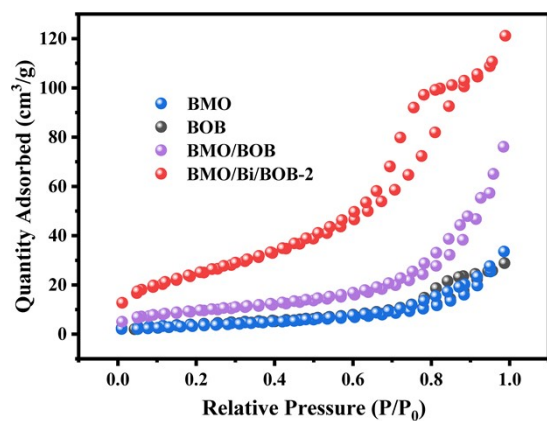


Figure S1. N_2 adsorption-desorption isotherms of BMO, BOB, BMO/BOB and BMO/Bi/BOB-2.

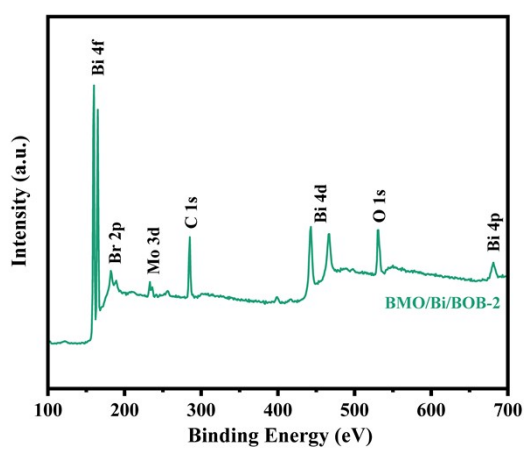


Figure S2. Survey XPS spectrum of BMO/Bi/BOB-2.

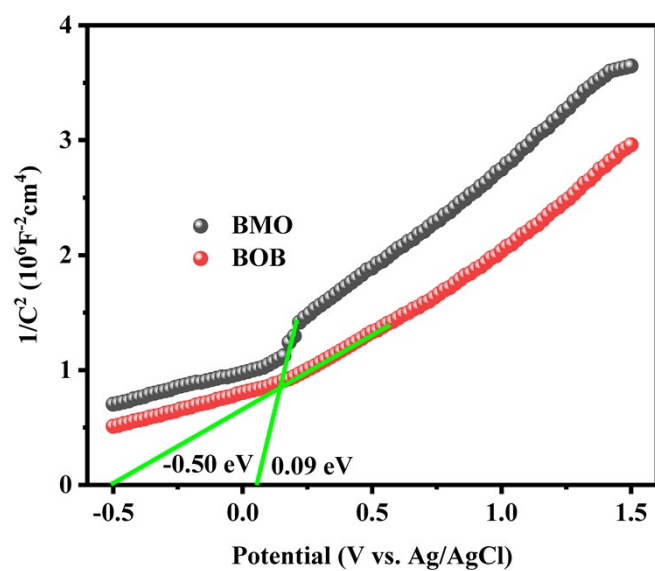


Figure S3. Mott-Schottky plots of BMO and BOB.

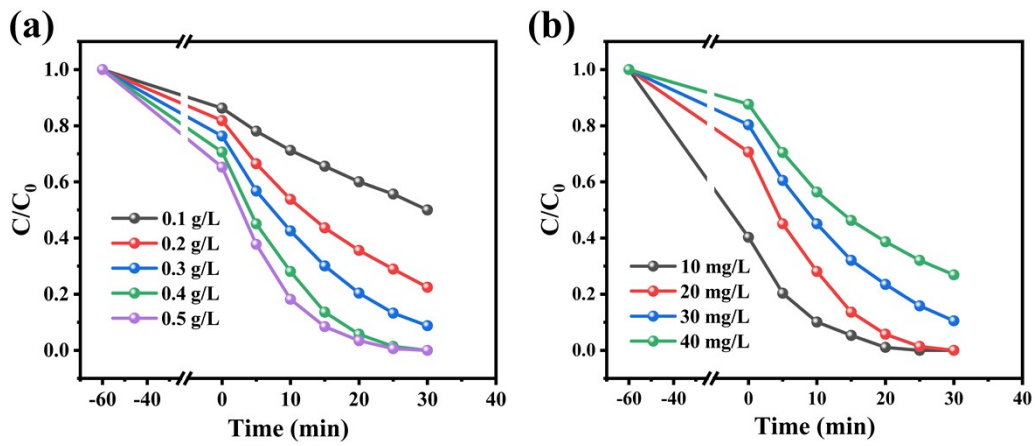


Figure S4. (a) Effects of BMO/Bi/BOB-2 dosage on photocatalytic CIP degradation process ($[CIP] = 20 \text{ mg/L}$); (b) Effects of CIP concentration on photocatalytic degradation process ($[BMO/Bi/BOB-2 \text{ dosage}] = 0.4 \text{ g/L}$).

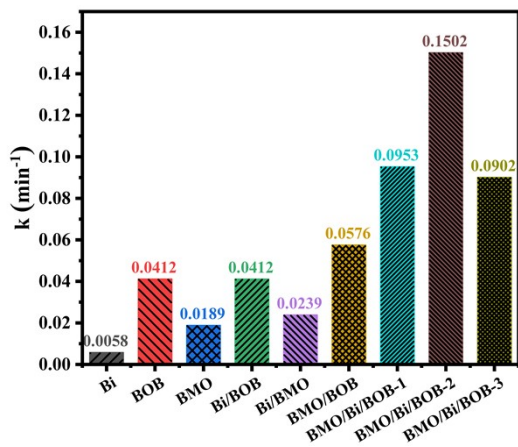


Figure S5. k values of as-prepared photocatalysts for CIP degradation.

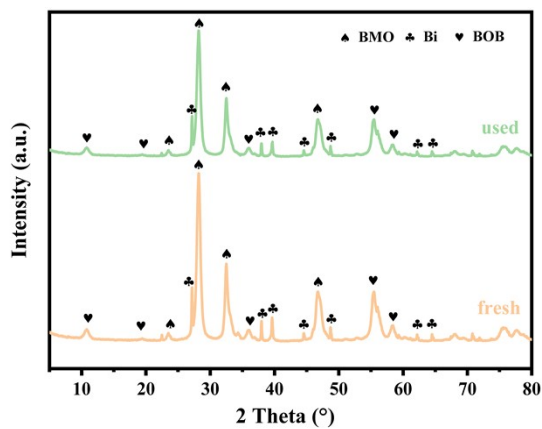


Figure S6. XRD patterns of fresh and used BMO/Bi/BOB-2.

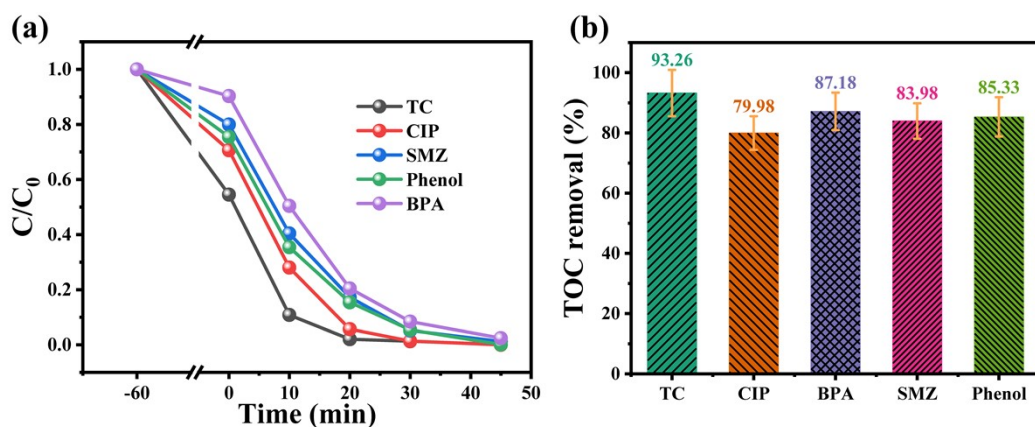


Figure S7. (a) The photocatalytic degradation curves and (b) TOC removal ratios of different organic pollutants by BMO/Bi/BOB-2.

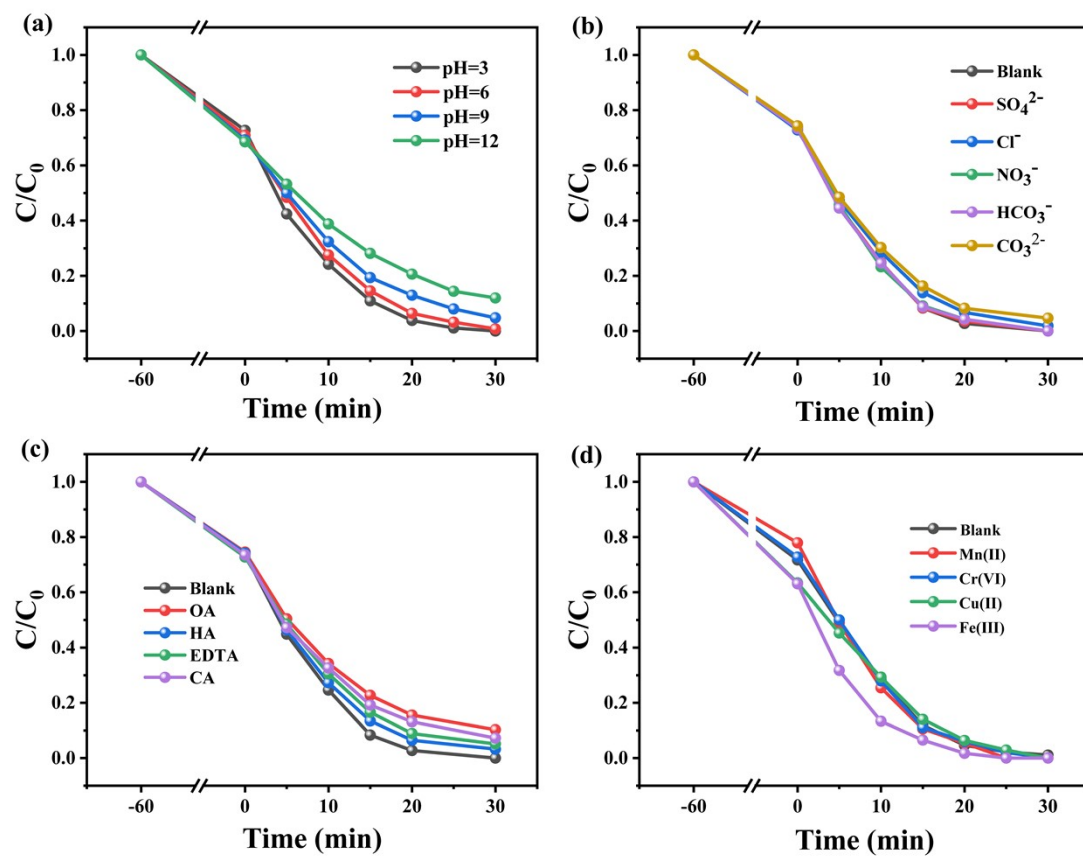


Figure S8. The effects of pH values (a), anions (b), organic matters (c), cations (d), on the degradation of CIP over BMO/Bi/BOB-2.

As shown in Fig. S8a, the photocatalytic CIP degradation process was gradually inhibited with the increase of pH value. At the high pH values, both of the CIP and photocatalyst were both negatively charged, leading to electrostatic repulsion between them and the low photocatalytic degradation efficiency of CIP. As shown in Fig. S8b-

d, we investigated the effect on photocatalytic CIP degradation of 5 common environmental coexist anions (SO_4^{2-} , Cl^- , NO_3^- , HCO_3^- and CO_3^{2-}), 4 common environmental coexist organic acids (OA, HA, EDTA and CA) and 4 common environmental coexist heavy metals (Mn^{2+} , CrO_4^{2-} , Fe^{3+} and Cu^{2+}). Among these environmental factors, 4 (Cl^- , NO_3^- , HCO_3^- and CO_3^{2-}) and 4 organic acids (OA, HA, EDTA and CA) exhibited a little negative effect on photocatalytic CIP degradation process, as they could act as trapping agents of $\cdot\text{OH}$. It's worth noting that Fe(III) could enhance photocatalytic CIP degradation process as Fe(III) could complex with CIP to form reddish brown photosensitive Fe(III)-CIP complexes.

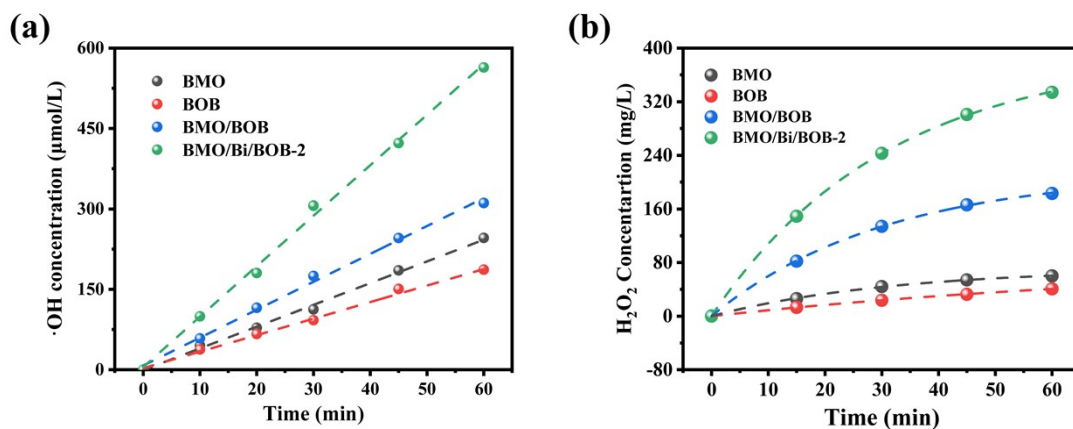


Figure S9. Photocatalytic $\cdot\text{OH}$ production curves (a) and H_2O_2 production curves (b) of BMO, BOB, BMO/BOB and BMO/Bi/BOB-2.

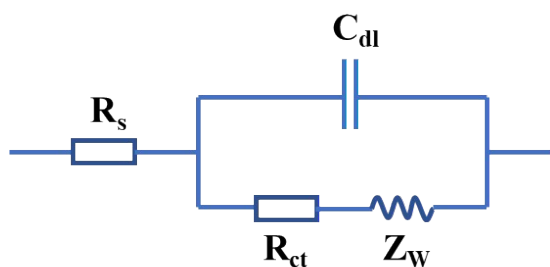


Figure S10. The analog equivalent circuit diagram of electrochemical impedance test

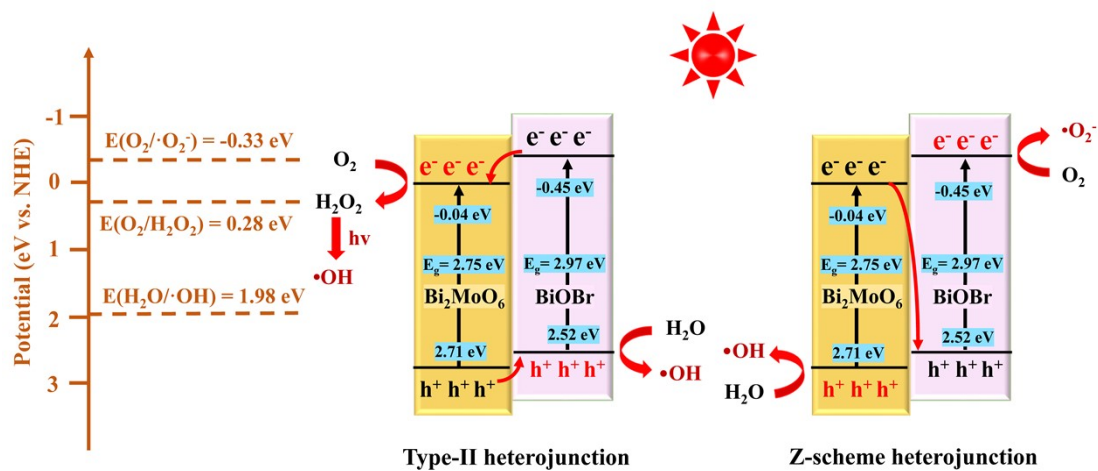


Figure S11. Schematic diagrams for type-II and Z-scheme heterojunction.

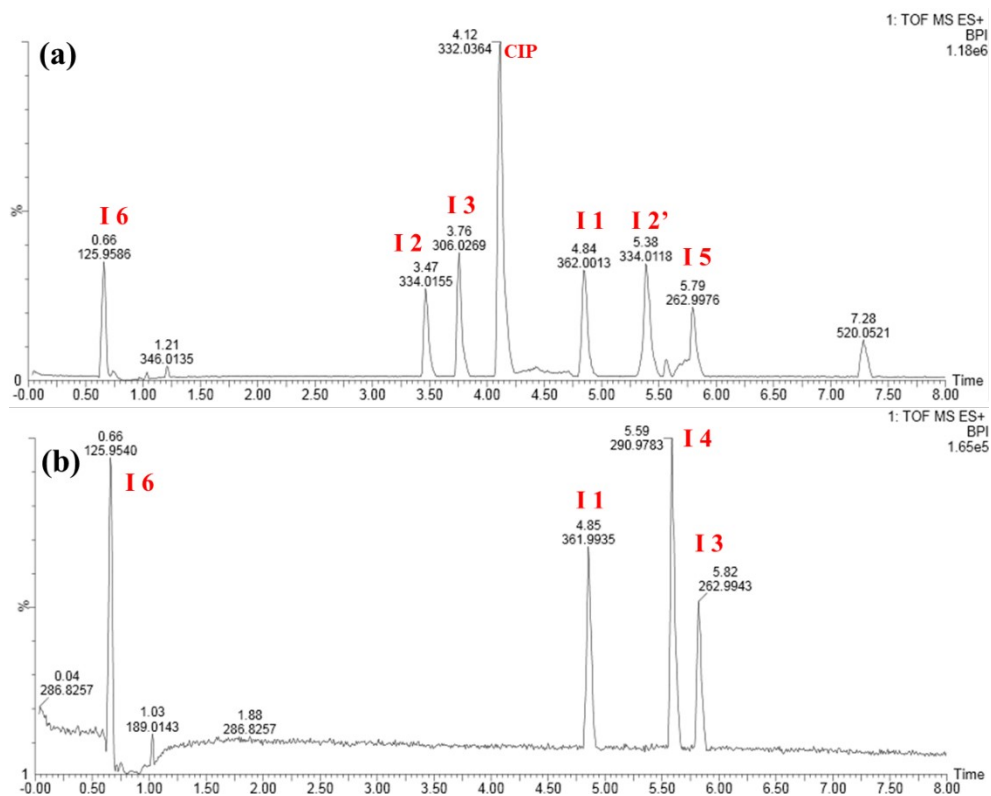


Figure S12. LC-MS chromatogram in ES⁺ mode for samples withdrawn at (a) 15 min and (b) 30 min irradiation.

References

1. X. Yu, J. Zhang, J. Zhang, J. Niu, J. Zhao, Y. Wei and B. Yao, Photocatalytic degradation of ciprofloxacin using Zn-doped Cu₂O particles: Analysis of degradation pathways and intermediates, *Chem. Eng. J.*, 2019, 374, 316-327.
2. F. Wang, X. Yu, M. Ge and S. Wu, One-step synthesis of TiO₂/γ-Fe₂O₃/GO nanocomposites for visible light-driven degradation of ciprofloxacin, *Chem. Eng. J.*, 2020, 384, 123381.
3. N. Li, J. Zhang, Y. Tian, J. Zhao, J. Zhang and W. Zuo, Precisely controlled fabrication of magnetic 3D γ-Fe₂O₃@ZnO core-shell photocatalyst with enhanced activity: Ciprofloxacin degradation and mechanism insight, *Chem. Eng. J.*, 2017, 308, 377-385.
4. Q. Wang, Y. Cui, R. Huang, L. Zhong, P. Yan, S. Zhang, Q. Zhao, D. Jiang, A. Tang and H. Yang, A heterogeneous Fenton reaction system of N-doped TiO₂ anchored on sepiolite activates peroxymonosulfate under visible light irradiation, *Chem. Eng. J.*, 2020, 383, 123142.
5. Z. Jia, T. Li, Z. Zheng, J. Zhang, J. Liu, R. Li, Y. Wang, X. Zhang, Y. Wang and C. Fan, The BiOCl/diatomite composites for rapid photocatalytic degradation of ciprofloxacin: Efficiency, toxicity evaluation, mechanisms and pathways, *Chem. Eng. J.*, 2020, 380, 122422.
6. M. Chen, J. Yao, Y. Huang, H. Gong and W. Chu, Enhanced photocatalytic degradation of ciprofloxacin over Bi₂O₃/(BiO)₂CO₃ heterojunctions: Efficiency, kinetics, pathways, mechanisms and toxicity evaluation, *Chem. Eng. J.*, 2018, 334, 453-461.
7. X. Hu, H. Zhao, Y. Liang and R. Chen, Energy level mediation of (BiO)₂CO₃ via Br doping for efficient molecular oxygen activation and ciprofloxacin photodegradation, *Appl. Catal. B: Environ.*, 2019, 258, 117966.
8. K. Wang, Y. Li, G. Zhang, J. Li and X. Wu, 0D Bi nanodots/2D Bi₃NbO₇ nanosheets heterojunctions for efficient visible light photocatalytic degradation of antibiotics: Enhanced molecular oxygen activation and mechanism insight, *Appl. Catal. B: Environ.*, 2019, 240, 39-49.
9. S. Shanavas, S. Mohana Roopan, A. Priyadharsan, D. Devipriya, S. Jayapandi, R. Acevedo and P. M. Anbarasan, Computationally guided synthesis of (2D/3D/2D) rGO/Fe₂O₃/g-C₃N₄ nanostructure with improved charge separation and transportation efficiency for degradation of pharmaceutical molecules, *Appl. Catal. B: Environ.*, 2019, 255, 117758.
10. Y. Li, Y. Fu and M. Zhu, Green synthesis of 3D tripyramid TiO₂ architectures with assistance of aloe extracts for highly efficient photocatalytic degradation of antibiotic ciprofloxacin, *Appl. Catal. B: Environ.*, 2020, 260, 118149.
11. S. Li, T. Huang, P. Du, W. Liu and J. Hu, Photocatalytic transformation fate and toxicity of ciprofloxacin related to dissociation species: Experimental and theoretical evidences, *Water Res.*, 2020, 185, 116286.
12. J. Zhao, Z. Zhao, N. Li, J. Nan, R. Yu and J. Du, Visible-light-driven photocatalytic degradation of ciprofloxacin by a ternary Mn₂O₃/Mn₃O₄/MnO₂ valence state heterojunction, *Chem. Eng. J.*, 2018, 353, 805-813.
13. A. Kumar, G. Sharma, M. Naushad, T. Ahamad, R. C. Veses and F. J. Stadler, Highly visible active Ag₂CrO₄/Ag/BiFeO₃@RGO nano-junction for photoreduction of CO₂ and photocatalytic removal of ciprofloxacin and bromate ions: The triggering effect of Ag and RGO, *Chem. Eng. J.*, 2019, 370, 148-165.